

# Flow and clogging behavior of a mixture of particles in a silo

Sukhada C. Bhure,<sup>1,2</sup> Pankaj Doshi,<sup>3, a)</sup> and Ashish V. Orpe<sup>1,2, b)</sup>

<sup>1)</sup> *CSIR-National Chemical Laboratory, Pune 411008 India*

<sup>2)</sup> *Academy of Scientific and Innovative Research (AcSIR), Ghaziabad 201002 India*

<sup>3)</sup> *Pfizer Research and Development, Pfizer Products India Private Limited, Mumbai 400051, India*

(Dated: 3 July 2024)

We investigated the clogging behavior observed during the flow of aspherical particles from a silo in the presence of spherical particles of different sizes and proportions using flow visualization experiments and discrete element method (DEM) simulations. The size of the avalanche, essentially the tendency of clogging, exhibits non-monotonic dependence on the spherical particle volume fraction. For small enough content of spherical particles, the clogging tendency intensifies, whereas it reduces rapidly for high enough spherical particle fractions, with a minimum in between. The non-monotonic behavior is observed to persist over for different spherical particle sizes. The overall behavior is shown to arise due to competing effects between the localized total particle fraction influencing avalanche strength and mean size of the particles exiting the silo, influencing the probability of arch formation.

## I. INTRODUCTION

The phenomena of clogging during the outflow of dry granular material from a silo, while interesting in itself, has also resulted in throwing up another interesting phenomena of unclogging of the clogged silo. While the former has been studied over several years<sup>1–6</sup>, the latter has garnered attention in recent times. It has been shown that the silo unclogging may be forced through air jet impinging or silo vibration<sup>7</sup>, by having multiple exit orifices<sup>8,9</sup>, or by placing inserts at suitable locations inside the silo<sup>10</sup>. These forcings can either break the stable arch or reduce the probability of arch formation in the first place, which is primarily responsible for clogging. Interestingly, the clogging-unclogging phenomena have also been extended to natural systems like movement of pedestrians or animals through a narrow exit<sup>11,12</sup> or artificial systems like the flow of colloidal particles through an orifice<sup>13</sup>.

Recently, it has been shown that the flow in a (2-dimensional) silo can be enhanced and clogging tendency be reduced due to presence of other (secondary) particles, which are smaller than the bulk particles, but are present at volume fractions as high as 0.2–0.4<sup>14,15</sup>. The silo was operated in the vibration mode, presumably to well mix two different sized particles. The probability of clog formation was found to be reduced due to the presence of secondary particles which led to the formation of an arch easily breakable due to vibration<sup>14</sup>. The presence of these particles also showed an increase in the overall flow rate with an optimal dependence on the particle size<sup>15</sup>. Our interest lies in understanding the effect of such secondary, smaller spherical particles on the clogging/flow behavior in the silo, but in small amounts, akin to the presence of trace impurities in the flow. In practice, the impurities

are bound to be present in the powder material, the effect of which on the flow or clogging is invaluable. Furthermore, we intend to study the flow and clogging behavior of aspherical particles, encountered mostly in practical situations. For simplicity, we consider the secondary particles to be spherical in shape. Apart from practical considerations, the study of the flow of non-spherical particles is fundamentally interesting in its own way. They are known to exhibit clogging characteristics differing from those observed for spherical particles. For instance, the breakdown of the exponential trail in avalanche distributions<sup>16</sup>, higher probability to form clogs due to possibility of multiple contact points and approach to spherical particle behavior with increased vertices in a polygon<sup>17,18</sup> are some of the peculiar observations related to non-spherical particle shape.

In this work, we focus on understanding the clogging and flow behavior of cylinder-shaped particles in the presence of small amounts of spherical particles in a 3-dimensional silo. We carry out the required study using flow visualization experiments and discrete element method (DEM) simulations. In Sec.II, we describe the experimental system and simulation details followed by results focusing on the avalanche size behavior and relevant characteristics of the system. Toward the end, we provide quantitative reasoning to explain the observed phenomena.

## II. METHODOLOGY

### A. Experimental details

Experiments are performed in a silo with dimensions as shown in Fig. 1. The side and bottom walls of the silo are made out of acrylic plates glued to each other, while the top is kept open to pour the granular material. The material outflows from an exit slit of fixed width. Two types of particles are used in the experiment. The bulk

<sup>a)</sup> Electronic mail: [pankaj.doshi@pfizer.com](mailto:pankaj.doshi@pfizer.com)

<sup>b)</sup> Electronic mail: [av.orpe@ncl.res.in](mailto:av.orpe@ncl.res.in)

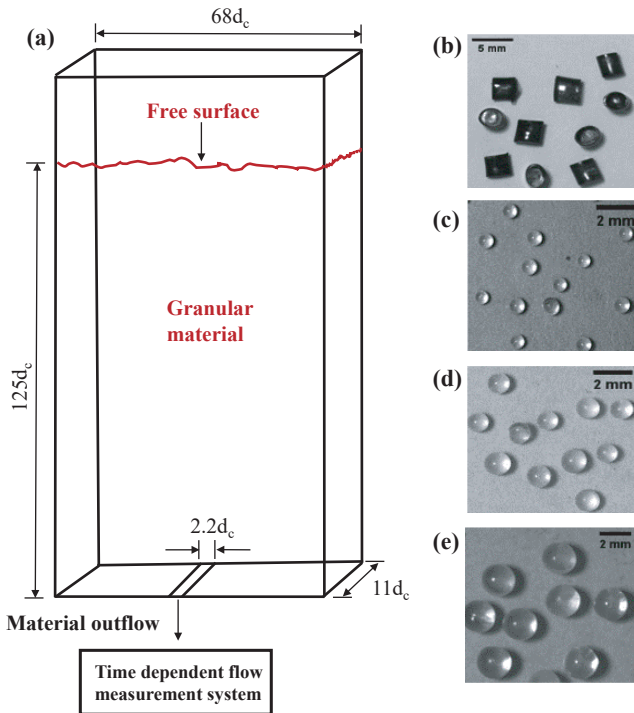


FIG. 1. (a) Schematic of experimental silo system (b) Cylinder-shaped bulk particle with equivalent sphere volume diameter  $d_c = 3.2$  mm. Spherical particles with diameters ( $d_s$ ) of 0.7 mm, 1.0 mm and 2.0 mm are shown, respectively, in (c), (d) and (e).

particles comprise of cylinders made from poly-methyl methacrylate (PMMA), of density 1.2g/cc, with an elliptical cross-section. The length of each cylinder is 3.1 mm, while the major and minor diameters are of length 3.2 mm and 2.2 mm, respectively. The diameter ( $d_c$ ) of an equivalent sphere volume is, then, calculated as 3.2 mm. Glass beads, of density 2.5g/cc and three different diameters ( $d_s$ ), viz., 0.7, 1 and 2 mm are used as secondary spherical particles resulting in particle size ratios ( $r = d_c/d_s$ ) of 4.6, 3.2 and 1.6 respectively. Images of these particles are shown in Figs. 1(b)-1(e).

For each experiment, the silo was filled with a mixture of bulk and one of the spherical particles up to a height of  $125d_c$ , while keeping the exit slit closed. The mixture was prepared by manual mixing of bulk cylindrical particles with predefined spherical particle volume fraction ( $\phi$ ) varied in the range 0-0.1. The mixture was, then, poured in the silo by employing distributed filling method. The outflow from the silo was initiated by opening the exit orifice, and the flowing material was collected directly on a weighing scale. Given the size of the orifice with respect to the bulk particle size, the orifice clogged after flowing for some time. The total mass, comprising both the particles, collected on the weighing scale till the occurrence of clogging was termed as the avalanche size ( $S$ ). After a wait time of 5s, the flow was reinitiated by piercing the exit arch with a pointed object to trigger

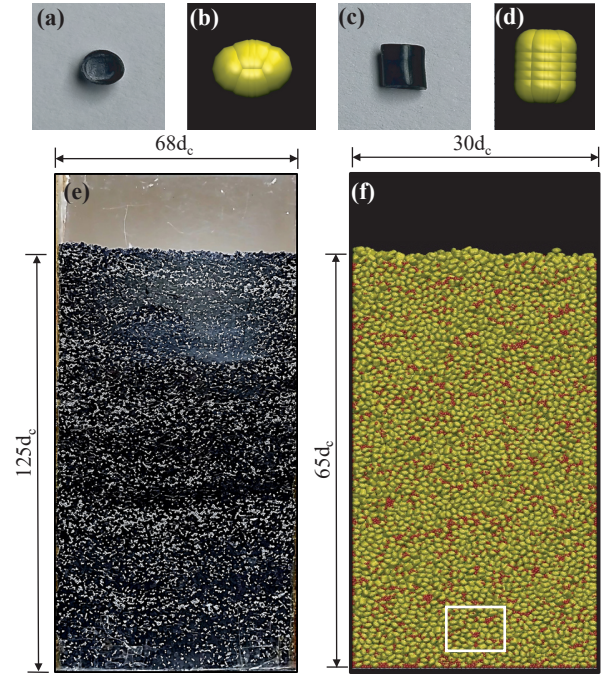


FIG. 2. Simulated particle and silo system. (a) Top view of the experimental particle. (b) Top view of the simulated particle. (c) Front view of the experimental particle. (d) Front view of the simulated particle. (e) and (f) represents the front view of the silo filled with a binary mixture of cylindrical and spherical particles, respectively in experiments and simulations, with  $\phi = 0.05$  and  $r = 3.2$ . The white box near the exit represents the region of interest for the requisite analysis as described later in the text.

another avalanche. The procedure was repeated till the fill height reduced to  $50d_c$ , following which the remainder of the material was emptied out, and the silo refilled back to a height of  $125d_c$  to restart the experiments. For every spherical particle concentration and size employed, the silo was filled about five times resulting in at least 500 independent avalanche events. The above procedure was repeated for different volume fractions and sizes of spherical beads.

## B. DEM simulations

The discrete element method (DEM) simulations were carried out to investigate the clogging of aspherical particles in the presence of secondary spherical particles. The simulations were carried out using an open source program, LIGGGHTS (LAMMPS Improved for General, Granular and Granular Heat Transfer Simulations), for different sphere volume fractions. The non-spherical particle (cylinder with elliptical cross section) was created using the in-built “multisphere” routine of the LIGGGHTS software. The approach involves clumping together predefined number of spheres of specific size. The resulting non-sphericity of the particle is dependent

on the number of clumped spheres, their location with respect to each other and the degree of overlap. Over here, we considered 50 spheres to generate a cylinder with elliptical cross section, while maintaining the relative magnitudes of the length, minor diameter, and major diameter the same as for the experimental particle. As seen from Figs. 2(b) and 2(d), the shape of the particle generated in simulations seems to be reasonably close to the experimental particle [see Fig. 1(b)], barring the sharp corners. A further increase in the number of spheres allowed for replicating the corners in a better manner, but required much longer simulation time. However, this did not alter the flow behavior significantly and, hence, was not considered. The secondary spherical particle was simply modeled as a sphere of prescribed size.

The silo of smaller size, viz. height  $65d_c$ , width  $30d_c$ , and depth  $10d_c$ , was used in simulation. Reduced dimensions of the silo were used to reduce the simulation time while ensuring the absence of wall effects. Moreover, the number and the size ratio of aspherical particles to spherical particles was kept the same as in experiments for a given sphere volume fraction. Figures 2(e) and 2(f) show the front view of the silo, respectively for experiments and simulations, comprising a mixture of particles ( $\phi = 0.05$ ) for a particle size ratio  $r = 3.2$ .

The simulation employs Hertzian contact model for calculation of force between two contacting particles. The Hertzian contact model was used in this work due to its ability to better capture the realistic behavior of granular materials, given the dependence of the interaction force on the overlapping area instead of overlapping distance considered in Hookean contact models<sup>19,20</sup>. The Hertzian model, thus, results in a more realistic force evolution and has been used previously quite frequently<sup>19-23</sup>. The contact force comprises of normal ( $F_n$ ) and tangential ( $F_t$ ) components, each of which includes two terms given as

$$\mathbf{F}_n = \left( k_n \delta \mathbf{n} - \frac{\gamma_n \mathbf{v}_n}{2} \right), \quad (1)$$

$$\mathbf{F}_t = - \left( k_t \Delta \mathbf{s}_t + \frac{\gamma_t \mathbf{v}_t}{2} \right), \quad (2)$$

where  $\mathbf{n}$  is the unit vector along the line connecting centers of two particles,  $\mathbf{v}_t$  and  $\mathbf{v}_n$  are, respectively, the tangential and normal components of particle velocities. Both, the normal elastic constant ( $k_n$ ) and tangential elastic constant ( $k_t$ ) are chosen to be of the order of  $10^7$   $mg/d_\alpha$ . The values of the normal damping term ( $\gamma_n$ ) and tangential damping term ( $\gamma_t$ ) are chosen to be of the order of  $10^2 \sqrt{g/d_\alpha}$ . Here,  $d_\alpha$  represents either  $d_c$  for cylindrical particles or  $d_s$  for spherical particles, and  $g$  represents gravity acting in downward direction. The value  $\Delta \mathbf{s}_t$  is the tangential displacement between two particles to satisfy the Coulomb yield criterion given by  $\mathbf{F}_t = \mu_s \mathbf{F}_n$ , where  $\mu_s$  is the coefficient of static friction coefficient. The density ratio between cylindrical bulk particles and spherical particles was maintained the same

TABLE I. Values of coefficient of static and rolling frictions for different contact pairs used in simulations

Contact pair	$\mu_s$	$\mu_r$
Cylinder-cylinder	0.9	0.2
Cylinder-sphere	0.7	0.15
Sphere-sphere	0.4	0.0

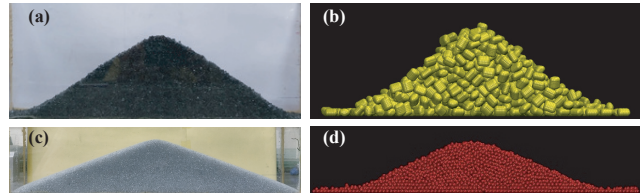


FIG. 3. Snapshot of the granular pile created for cylindrical particles in (a) experiments and (b) simulations and for spherical particles in (c) experiments and (d) simulations for particle size ratio ( $r$ ) of 3.2.

as in experiments. The integration time step used in the simulation is  $10^{-4}$ . The silo was filled with mixture up to a height of  $65d_c$ , and the flow in simulations was initiated by opening the exit slit. The total mass of particles flowing out of the silo before the orifice clogged was termed as the avalanche size ( $S$ ). The flow was reinitiated by removing a few particles in the arch. This procedure was repeated till the fill height reduced to  $40d_c$ . This resulted in about 70 independent avalanche events. However, unlike that in experiments, the silo was not refilled to record more number of avalanche events as that became computationally prohibitive. However, as shown later, about 70 recorded avalanche events per case seems reasonably large enough to capture the observed experimental phenomena.

### C. Parameter calibration

The calibration of the simulation parameters to match the experiments can be an uphill task given the range of parameters used and two types of particles and materials employed. For simplicity, except friction coefficients, all the remaining contact model parameters are of the same order of magnitude, typically as used previously<sup>24,25</sup>, but for glass beads<sup>9,24,26</sup> which has a modulus about an order of magnitude greater than PMMA. Note that these values of the contact model parameters are substantially lower than those relevant to real glass and are chosen so as to reduce the overall computational effort<sup>9,27</sup>. In addition to the coefficient of static friction ( $\mu_s$ ), we have also employed coefficient of rolling friction ( $\mu_r$ ) between the particles. The latter represents the ease with which the particles roll past one another and will be determined by the asphericity of the particles in contact. Typically, for the sphere-sphere contact, the value can be expected to be quite low, while it can be high for the cylinder-cylinder



contact. The values of both the friction coefficients were adjusted so as to match the value of static angle of repose measured from simulations to that measured from experiments.

The material, either cylinders or spheres, were slowly poured in a rectangular cell to form a static heap. The length, height, and depth of the experimental cell was  $150d_c$ ,  $65d_c$ , and  $18d_c$ , respectively, while that of simulation cell was  $30d_c$ ,  $15d_c$ , and  $10d_c$ , respectively. The cell dimensions were sufficiently large to prevent any kind of end effects. In experiments, the static image of the heap was captured using a digital camera positioned sideways and orthogonal to the sidewall of the rectangular cell [see Figs. 3(a) and 3(c)]. In simulations, the angle was measured from the final static position of the particles exported as an image [see Figs. 3(b) and 3(d)]. In each image, a central, nearly flat free surface region of the heap (about  $15d$ ) was analyzed to obtain the angle of repose. Every experimental measurement was repeated about six times to ensure consistency. The values of friction coefficients reported in Table I, averaged over all spherical particle sizes, correspond to the scenario wherein the angle measured for an experimentally prepared pile varies within half a degree from that measured in a pile from simulations. This close agreement suggests that the finalized simulation parameters seem reasonable enough to qualitatively reproduce experimental observations and were used in carrying out simulations of particles flowing out of silo.

### III. RESULTS & DISCUSSION

In the following, we first provide a qualitative understanding from the observations. This is then followed by a quantitative discussion of the clogging behavior in terms of avalanche size variations as observed in experiments and compared with those observed in simulations. Toward the end, we discuss about certain specific measurements from the simulation data, which have been used to explain the experimental observations.

Figure 4 shows images acquired in experiments during an avalanche at different times and for three different volume fractions ( $\phi$ ) of spherical particles of diameter  $d_s = 1$  mm, i.e.,  $r = 3.2$ . The images show particle configurations at different stages of an avalanche in the vicinity of the exit orifice near the front wall of the silo. The video representation of these images for different sphere volume fractions and sizes is available as a supplementary material. In each case, as seen from the respective videos, the overall motion appears intermittent, eventually leading to an arch formation and clogging. The number of small spheres increase with increasing sphere concentration, though the distribution is not uniform. The spheres, appearing as distinct and small clusters, seem to fill in the voids created by the packing of cylinders. The number of clusters increase with increasing packing fraction, though the size of the cluster remains nearly the same.

This is suggestive of the upper limit for the void space available for filling due to smaller spherical particles. The formation of the arch and its shape does not seem to depend on the spherical particle fraction, underlining the random nature of the event in all cases. Near identical, qualitative behavior is also observed for other spherical particle fractions and sizes.

The simulation counterpart for the earlier discussion on experimental observations is shown in fig. 5. The images are acquired from three different view positions to understand the 3-dimensional nature of the flow and clogging. Unlike in fig. 4, the images in fig. 5 are only shown for the final clogged state. The flow of the avalanches leading to clogging, however, can be seen from the videos available as the supplementary material for different particle fractions and sizes. The main qualitative features seen in experiments, i.e., increased number of smaller spheres with increased fractions, formation of clusters are observed in simulations too. There is, however, a hint of the occurrence of segregation near the bottom, not seen clearly in experiments. The corresponding view from the sidewall (second panel in the figure) shows similar configuration of spherical particles and cylinders showing that the behavior is not a localized, but rather a bulk phenomenon. The perspective view in third panel in Fig. 5 shows the complicated nature of the arch across the depth of the silo. The occurrence of the flow even when the particles near the front wall are stationary is a direct consequence of this 3-dimensional nature of the arch formation.

While the images in figs. 4 and 5 and corresponding videos show the behavior for one spherical particle size, a similar qualitative behavior is also observed for other spherical particle sizes. From all these observations, it can be anticipated that the presence of spherical particles in the voids, individually or in clusters, may influence the flowability of the system and arch forming tendency. However, these can be quantitatively ascertained by measurement of the mean and distribution of the avalanche sizes and their dependence on spherical particle size and fractions as discussed next.

The avalanche size represents the amount of material flowing out of silo till the orifice is clogged. The avalanche size ( $S$ ) in experiments is the total mass of cylindrical and spherical particles collected during the flow before the occurrence of clog. The average value ( $\langle S \rangle$ ) is obtained over 500 independent flow (or clogging) events. The variation of normalized average avalanche size ( $\langle S \rangle / \langle S_0 \rangle$ ) with the spherical particle concentration ( $\phi$ ) is shown in fig. 6(a). Here,  $S_0$  represents the avalanche size for the base case, i.e., in the absence of spherical particles ( $\phi = 0.0$ ). Several interesting features are evident from this figure, which we dwell upon next.

The magnitude of the avalanche size is governed by the ability of the flowing particles to form a stable arch. The increased avalanche size represents longer flow duration before clogging takes place, indicating a lesser tendency to form a stable arch and vice versa for decreased

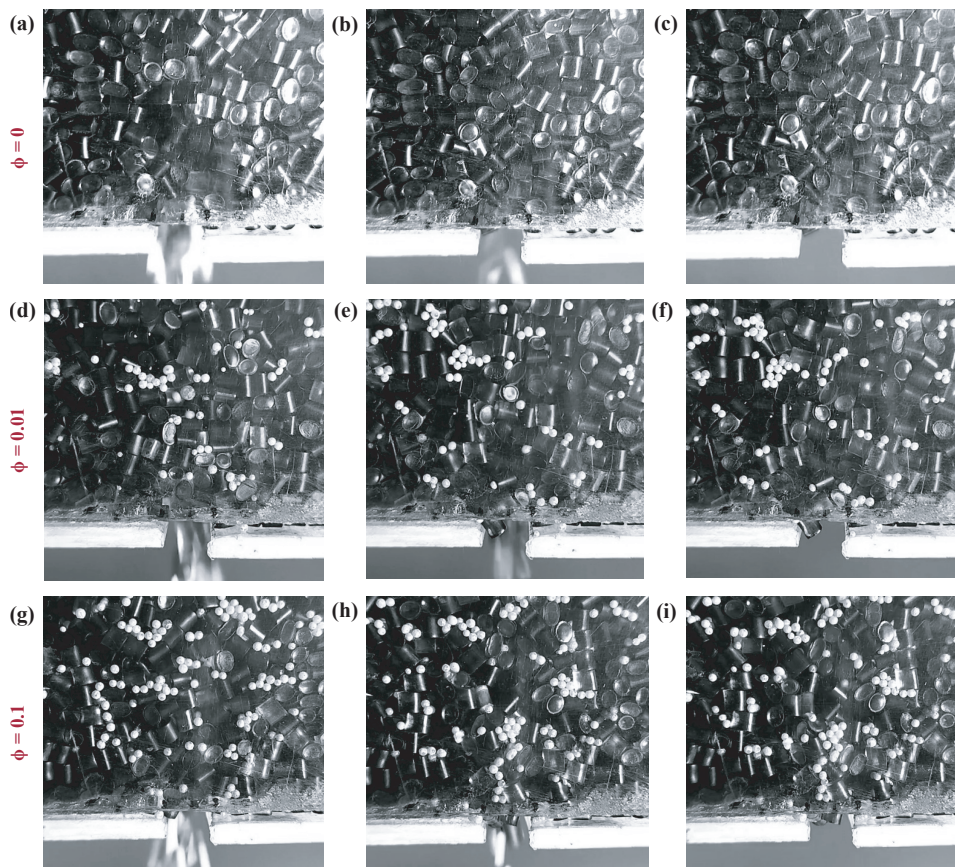


FIG. 4. Images from experiments showing particle configurations during flow and arch formation in the vicinity of the silo exit for a few different fractions of spherical particles ( $r = 3.2$ ). Spheres are seen as white circles in the images. All the images are acquired at the front wall.

avalanche sizes. In the limit of infinite avalanche size (when flow never stops), the tendency of arch formation will be negligible, and, in the limit of no flow or immediate clogging, the tendency will be quite high. It may be intuitively expected that the presence of small spherical particles may lubricate the flow of cylindrical particles and/or may reduce direct contacts between cylinders thereby reducing the tendency of arch formation, resulting in increased avalanche size. However, as seen from Fig. 6(a), the observed behavior is exactly the opposite. The presence of small spherical particles actually reduces the avalanche size compared to the base case, essentially aiding the clogging behavior. The decrease in the avalanche size is, however, observed over a limited range of sphere volume fraction, leading to a minimum in the avalanche size at an intermediate sphere volume fraction, which is dependent on the size of spherical particle. Any further addition of spherical particles increases the avalanche size, i.e., inhibits clogging tendency.

For higher values of  $\phi$ , the avalanche size seems to increase rapidly, similar to that observed previously<sup>14,15</sup>. This can be expected as, with increasing volume fraction of spherical particles in the system, the proportion of these particles within the total number of particles ex-

iting the silo will also increase. Given much larger orifice size relative to the size of spherical particles, they cannot be expected to form an arch. Moreover, their presence in large numbers will also reduce the mean size of particles exiting the silo, thereby reducing the tendency of forming an arch, the result being a larger avalanche size. Indeed, the avalanche size will diverge at high enough spherical particle concentration approaching  $\phi = 1.0$ , wherein there will be primarily spherical particles in the outflow thereby precluding arch formation and hence no clog formation. While the overall (non-monotonic) behavior remains same for different sizes of spherical particles, certain deviations exist, which are not quite systematic and hence difficult to understand at this time. For instance, the minimum avalanche size spreads over a range of spherical particle fractions for smallest size spherical particle ( $r = 4.6$ ) [(see Fig. 6(a)], while the spread is limited to a narrow range of fractions for the other two size ratios.

The equivalent data as acquired from DEM simulations is shown in Fig. 6(b) for the same three particle size ratios as in experiments. While the data for  $r = 3.2$  and  $r = 1.6$  is nearly the same as that obtained in experiments, qualitative differences are seen for the case of



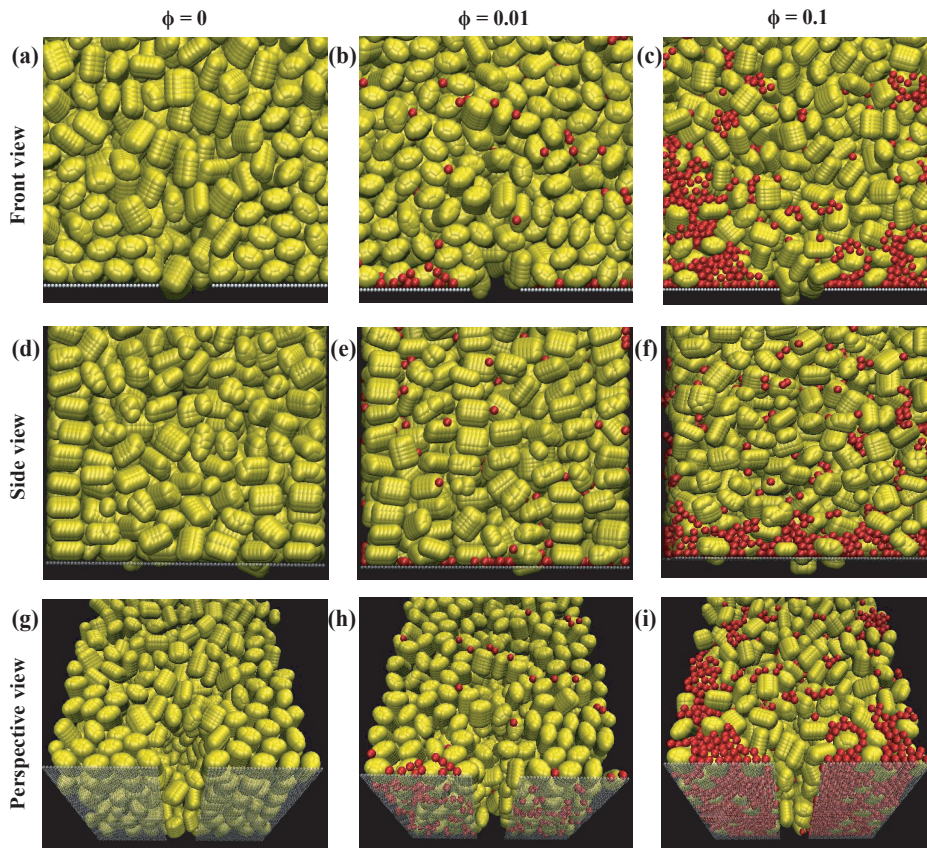


FIG. 5. Images from simulations showing particle arrangements in the vicinity of the silo exit for a few different fractions of spherical particles ( $r = 3.2$ ) after the flow has clogged. Images in the first panel (a-c) are acquired near the front wall. Images in second panel (d-f) are acquired near one of the side walls. Images in the third panel (g-i) are acquired from the bottom at a perspective angle to the silo. The shaded region in the third panel represents the bottom plate with a slit in between.

smallest sphere of  $r = 4.6$  compared with experiments. The more sustained minimum observed in experiments is not seen in simulations (see Fig. S1 provided in the supplementary material for better comparative representations). This disparity in the observations for different spherical particle sizes, in experiments as well as simulations, can be possibly attributed to the lack of exact replication of (i) the shape of cylindrical particle in simulations, particularly the sharp edges and (ii) actual inter-particle interaction. This inadequacy seems to have a different effect with respect to spherical particle concentration and size, the origins of which are not clear at the moment. However, more importantly, the non-monotonic variation of normalized avalanche size with spherical particle volume fraction is exhibited for all the three sphere sizes, suggestive that the physics behind the experimental observations is captured quite well in simulations. In that case, the more detailed and the three dimensional simulation data can, then, be used for explanation of the observations as discussed later.

The distributions of avalanches exhibit exponential behavior for all the cases as shown in Fig. 7. The exponential decay represents random nature of discrete avalanche events as has been shown previously in previous stud-

ies<sup>5,7-9,16</sup>. This suggests that the presence of spheres does not influence the inherent random nature of the clogging phenomena. However, the length scale of the exponential decay is different for experiments and simulations. Near-similar qualitative behavior is obtained for remaining sphere volume fractions as well as for different spherical particle sizes.

As discussed earlier, the increase or decrease in the avalanche size will be governed by the probability of clogging occurrence, which in turn will depend on probability of arch formation subject to the local flow conditions prevailing near the silo exit. In a recent work<sup>25</sup>, it was shown that the clogging occurrences reduced monotonically with increased translational kinetic energy in the system, which was increased by increasing the driving (gravity) force and increasing the orifice width. The authors assumed that for small enough translational kinetic energy, i.e., slow enough flow, the formed arch is able to resist its breakage till the flow eventually stops. The exact reverse happens for fast flows, wherein the arch is unable to prevent its breakage, thereby reducing the chances of clogging.

We borrow the same argument over here to explain our observations. However, the possible drivers for alter-

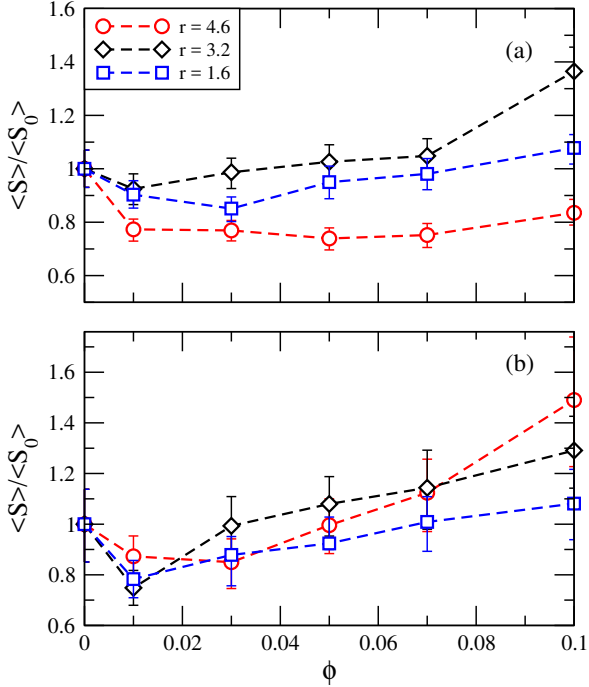


FIG. 6. Variation of normalized average avalanche size ( $\langle S \rangle / \langle S_0 \rangle$ ) with spherical particle volume fraction ( $\phi$ ). Data from (a) experiments and (b) simulations for three different particle size ratios ( $r$ ).  $\langle S_0 \rangle$  represents average avalanche size in the absence of spherical particles. Error bars represent confidence interval of 95%.

ing the kinetic energy over here are the spherical particle concentration and size ratio, while maintaining the gravitational force and orifice width constant. Under these circumstances, the only possible way for increase or decrease in the kinetic energy is the variation of the packing fraction in the system. We have calculated the packing fraction during the flow in a box of length  $10d_c$ , width  $10d_c$ , and depth  $10d_c$ , located about  $3.5d_c$  above the exit orifice [shown in Fig. 2(f)]. The location of the box represents the region closest to the orifice, which can be expected to exert maximum influence, while also away from the actual arch formation location, which typically ranges in the region up to  $3d_c$  above the orifice. The volume fraction in the box was obtained as an average over all the particles across all avalanches and also over all times within each avalanche. It is to be noted that over the entire avalanche duration, the volume fraction measured within the region varied up to 0.5% of the initial value when the avalanche was initiated. Thus, the average value reflects the packing state during the flow for a specified spherical particle concentration and size ratio, which, we believe, should influence the average kinetic energy of the system. We consider both, the translational component of kinetic energy ( $k_{te}$ ), which accounts for the flow speed of all particles, and the rotational component of the kinetic energy ( $k_{re}$ ), which predominantly represents the ability of the cylindrical particles, to orient

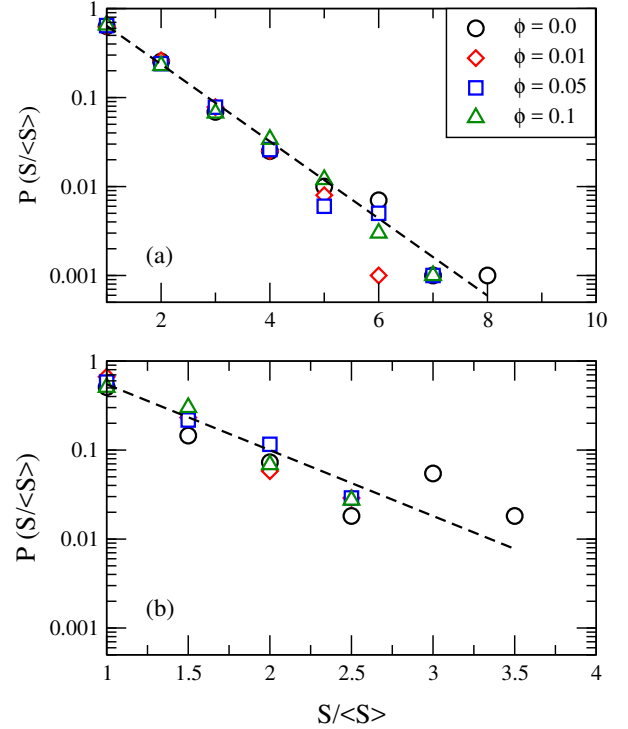


FIG. 7. Probability distribution of normalized avalanche size ( $S / \langle S \rangle$ ) for size ratio ( $r = 3.2$ ) and different spherical particle volume fraction in (a) experiments and (b) simulations. The dashed line represents an exponential fit.

themselves appropriately. The latter quantity can be expected to correlate with the average angle of orientation ( $\theta$ ) of the cylindrical particles, calculated with respect to the vertical (or flow direction).

Figure 8(a) shows the variation of the average total volume fraction ( $\langle \phi_t \rangle$ ) and normalized average translational kinetic energy ( $\langle k_{te} \rangle / \langle k_{te0} \rangle$ ), normalized average rotational kinetic energy ( $\langle k_{re} \rangle / \langle k_{re0} \rangle$ ), and average angle of orientation of cylinders with vertical ( $\langle \theta \rangle$ ) with spherical particle volume fraction ( $\phi$ ) in the region of interest. Here,  $k_{te0}$  and  $k_{re0}$  correspond to the avalanche for the base case, i.e., in the absence of spherical particles ( $\phi = 0.0$ ). Overall, the total volume fraction (including spheres as well as cylinders) will vary between the lower limit [ $\langle \phi_t \rangle = 0.509$ , shown as magenta line in Fig. 8(a)] in the absence of spherical particles and upper limit [ $\langle \phi_t \rangle = 0.59$  shown as orange line in Fig. 8(a)] in the absence of cylindrical particles (or only spherical particles). This is not surprising given the fact that only spheres are expected to pack efficiently than only cylinders. The average total volume fraction [shown as green squares in Fig. 8(a)] increases quickly for the lower values of spherical particle concentration followed by a gradual increase at corresponding higher values.

The initial rapid increase in the average total volume fraction ( $\langle \phi_t \rangle$ ) can be envisioned as the spherical particles filling the available voids between cylinders thereby

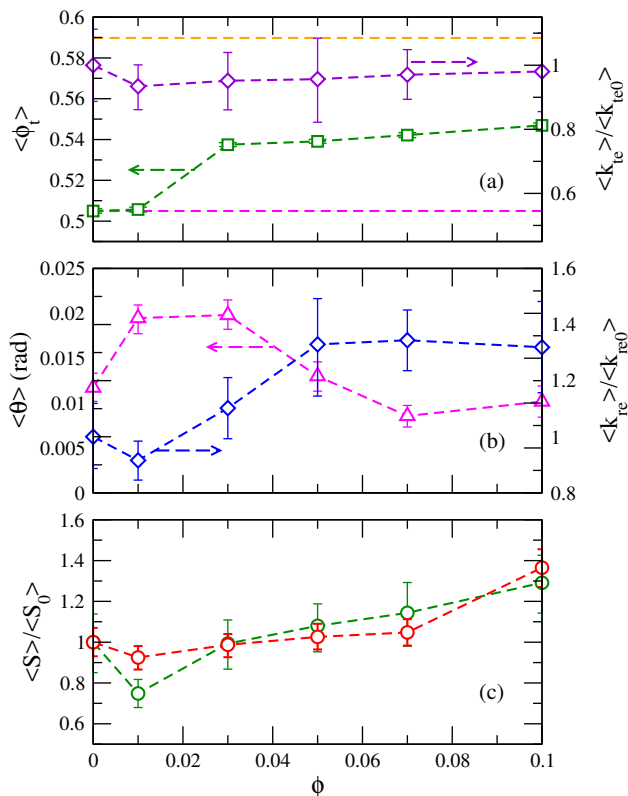


FIG. 8. (a) Variation of total (spheres and cylinders) average volume fraction ( $\langle\phi_t\rangle$ , green squares) and normalized average translational kinetic energy ( $\langle k_{te}\rangle/\langle k_{te0}\rangle$ , violet diamonds) of flowing particles with spherical particle volume fraction ( $\phi$ ). The dashed magenta colored line and orange colored line, respectively, represent the volume fraction during flow of only cylinders and only spherical particles. (b) Variation of average angle of orientation of the cylinders with vertical ( $\langle\theta\rangle$ , magenta triangles) and normalized average rotational kinetic energy ( $\langle k_{re}\rangle/\langle k_{re0}\rangle$ , blue diamonds) of flowing particles with spherical particle volume fraction ( $\phi$ ) (c) Variation of normalized average avalanche size ( $\langle S\rangle/\langle S_0\rangle$ ) with spherical particle volume fraction ( $\phi$ ) measured experimentally (red circles) and in simulations (green circles). The data is obtained for a size ratio of  $r = 3.2$ . Error bars represent confidence interval of 95%

improving the packed state. This progressive increase in the value of volume fraction is expected to gradually decrease the flow velocity leading to the decrease in the average translational kinetic energy ( $\langle k_{te}\rangle/\langle k_{te0}\rangle$ ) as indeed seen in Fig. 8(a). Second, the increased volume fraction will impede the ability of the cylindrical particles to rotate and align themselves with the flow direction, thereby reducing the average rotational kinetic energy ( $\langle k_{re}\rangle/\langle k_{re0}\rangle$ ) as seen in fig. 8(b). The direct consequence seems to be the increase in the average orientation angle ( $\langle\theta\rangle$ ) with respect to the vertical (flow) direction [see Fig. 8(b)]. The higher the orientation angle of cylinders with respect to vertical, higher would be the resistance to flow, while the minimum resistance can be expected when

cylinders align parallel to the flow direction. The combined effect of these three entities ( $k_{te}$ ,  $k_{re}$ , and  $\theta$ ) is to make the arch increasingly resistant to the flow, thereby leading to more frequent clogging and, hence, the reduction in avalanche size, in agreement with the previously published work<sup>25</sup>. This is observed in Fig. 8(b), wherein the decrease in the avalanche size (shown as green curve) coincides with the decrease in both the components of kinetic energy [violet curve in fig. 8(a) and blue curve in fig. 8(b)] and increase in average orientation angle with respect to vertical [magenta curve in Fig. 8(b)]. The minimum avalanche size is obtained for a spherical particle fraction corresponding to minimum in both components of kinetic energy, maximum in the orientation angle as well as the transition between rapid and slow increase in total volume fraction. This transition point represents the changeover from a state of higher clogging occurrences to a state of lower clogging occurrences.

Following the transition point, the total volume fraction increases gradually with increase in spherical particle fraction. Given that the total number of voids available are limited and mostly filled up, further increase in  $\phi$  simply adds up the number of spherical particles leading to a gradual change in total volume fraction. In view of the argument in the preceding paragraph, this should lead to further decrease in the value of kinetic energy. On the contrary, both the components of kinetic energy are seen to increase continuously. As already discussed, the relative proportion of small sized spherical particles increases in the material flowing out of the orifice, leading to a progressive decrease in the mean particle diameter (number average of cylindrical and spherical particles) with increasing value of  $\phi$ . The ratio of the orifice width to this mean particle diameter increases progressively, thereby reducing the probability of arch formation, leading to reduced clogging or increased avalanche size and consequently faster flow, and hence larger translational kinetic energy. The faster flow, perhaps, enables the cylinders to rotate more easily and orient themselves with the flow direction, thereby reducing the angle with the vertical and increase in the rotational kinetic energy. The observed non-monotonic dependence of avalanche size on spherical particle fraction is, then, due to competing effects between increased packing influencing the avalanche strength and reduced probability of arch formation with decreased mean particle size in the outflow zone. Nearly similar qualitative behavior is also observed for other two size ratios (not shown).

#### IV. CONCLUSIONS

The flow of cylindrical particles through a 3-dimensional silo is investigated in the presence of spherical particles present in different proportion and of different sizes. Flow visualization experiments and discrete element method (DEM) simulations are employed for this study. The clogging behavior is studied for an exit orifice



(or slit) of fixed size and is measured in terms of the size of an avalanche emanating from the silo.

The presence of spherical particle exhibits a non-monotonicity in the variation of avalanche size. For small enough spherical particle fraction, the avalanche size decreases, i.e., the clogging tendency increases, which is somewhat non-intuitive in nature and in contrast to previous observations<sup>14,15</sup>. However, for large enough tracer fraction the avalanche size increases rapidly, i.e., the clogging tendency decreases in agreement with previous observations<sup>14,15</sup>. Similar, qualitative, behavior is observed for all the spherical particle sizes used, though with certain quantitative differences arising out of size differences.

The non-monotonic behavior of clogging tendency is attributed to two effects arising due to addition of spherical particles, viz. increase in total particle fraction and reduced mean particle size exiting the orifice. For small enough spherical particle fractions, the former effect dominates, leading to reduced kinetic energy and increasingly resistive arch formation. At larger fractions, the latter effect dominates leading to faster flows, increased kinetic energy, and reduced clogging tendency.

It is quite interesting to know that such small presence of spheres, which typically may be neglected, can lead to unexpected clogging, not quite expected. The knowledge of the existence of such behavior would be of substantial interest to several industries handling powders in various applications. Fundamentally, the presence of such behavior can spur detailed modeling to understand the flow of bi-disperse granular material through the silo, something which is rarely studied. More interesting would be to study the carryover of this phenomena for particles of different shapes and for cohesive grains encountered in practice.

## ACKNOWLEDGMENTS

A.V.O gratefully acknowledges the financial support from the Science and Engineering Research Board, India (Grant No. CRG/2019/000423). S.C.B acknowledges the Council of Scientific and Industrial Research (CSIR), India, for the CSIR-GATE fellowship. The support and the resources provided by “PARAM Brahma Facility” under the National Supercomputing Mission, Government of India at the Indian Institute of Science Education and Research (IISER), Pune is gratefully acknowledged. The authors also gratefully acknowledge the computational resources provided by “Einstein cluster facility” at CSIR - National Chemical Laboratory, Pune.

<sup>1</sup>K. To, P. Y. Lai, and H. K. Pak, *Phys. Rev. Lett.* **86**, 71 (2001).

<sup>2</sup>J. Tang and R. P. Behringer, *Chaos* **21**, 041107 (2011).

<sup>3</sup>S. Tewari, M. Dichter, and B. Chakraborty, “Signatures of incipient jamming in collisional hopper flows,” *Soft Matter* **9**, 5016 (2013).

<sup>4</sup>C. C. Thomas and D. J. Durian, “Geometry dependence of the clogging transition in tilted hoppers,” *Phys. Rev. E* **87**, 052201 (2013).

<sup>5</sup>I. Zuriguel, “Clogging of granular material in bottlenecks,” *Pap. Phys.* **6**, 060014 (2014).

<sup>6</sup>C. C. Thomas and D. J. Durian, “Intermittency and velocity fluctuations in hopper flows prone to clogging,” *Phys. Rev. E* **94**, 022901 (2016).

<sup>7</sup>A. Janda, D. Maza, A. Garcimartín, E. Kolb, J. Lanuze, and E. Clément, “Unjamming a granular hopper by vibration,” *Eur. Phys. Lett.* **87**, 24002 (2009).

<sup>8</sup>A. Kunte, P. Doshi, and A. V. Orpe, “Spontaneous jamming and unjamming in a hopper with multiple exit orifices,” *Phys. Rev. E (Rapid Comm.)* **90**, 020201(R) (2014).

<sup>9</sup>A. V. Orpe and P. Doshi, “Friction-mediated flow and jamming in a two-dimensional silo with two exit orifices,” *Phys. Rev. E* **100**, 012901 (2019).

<sup>10</sup>I. Zuriguel, A. Janda, A. Garcimartín, C. Lozano, R. Arévalo, and D. Maza, “Silo clogging reduction by the presence of an obstacle,” *Phys. Rev. Lett.* **107**, 278001 (2011).

<sup>11</sup>I. Zuriguel, D. R. Parisi, R. C. Hidalgo, C. Lozano, A. Janda, P. A. Gago, J. P. Peralta, L. M. Ferrer, L. A. Pugnali, E. Clément, D. Maza, I. Pagonabarraga, and A. Garcimartín, “Clogging transition of many-particle systems flowing through bottlenecks,” *Sci. Rep.* **4**, 7324 (2014).

<sup>12</sup>I. Zuriguel, A. Janda, R. Arévalo, D. Maza, and A. Garcimartín, “Clogging and unclogging of many-particle systems passing through a bottleneck,” *EPJ Web. Conf.* **140**, 01002 (2017).

<sup>13</sup>R. C. Hidalgo, A. G. ni Arana, A. Hernández-Puerta, and I. Pagonabarraga, “Flow of colloidal suspensions through small orifices,” *Phys. Rev. E* **97**, 012611 (2018).

<sup>14</sup>A. Nicolas, M. N. Kuperman, and S. Bouzat, “A counterintuitive way to speed up pedestrian and granular bottleneck flows prone to clogging: can ‘more’ escape faster,” *J. Stat. Mech.*, 083403 (2018).

<sup>15</sup>M. A. Madrid, C. M. Carlevaro, L. A. Pugnali, M. Kuperman, and S. Bouzat, “Enhancement of the flow of vibrated grains through narrow apertures by addition of small particles,” *Phys. Rev. E* **103**, L030901 (2021).

<sup>16</sup>I. Zuriguel, A. Garcimartín, D. Maza, L. A. Pugnali, and J. M. Pastor, “Jamming during the discharge of granular matter from a silo,” *Phys. Rev. E* **71**, 051303 (2005).

<sup>17</sup>E. Goldberg, C. M. Carlevaro, and L. A. Pugnali, “Flow rate of polygonal grains through a bottleneck: Interplay between shape and size,” *Pap. Phys.* **7**, 070016 (2015).

<sup>18</sup>E. Goldberg, C. M. Carlevaro, and L. A. Pugnali, “Effect of grain shape on the jamming of two-dimensional silos,” *EPJ Web. Conf.* **140**, 06009 (2017).

<sup>19</sup>C. Thornto, S. J. Cummins, and P. W. Cleary, “An investigation of the comparative behaviour of alternative contact force models during elastic collisions,” *Powder Technol.* **210**, 189–197 (2011).

<sup>20</sup>S. B. Yeom, E. Ha, M. Kim, S. H. J. an S. Hwang, and D. H. Choi, “Application of the discrete element method for manufacturing process simulation in the pharmaceutical industry,” *Pharmaceutics* **11**, 414 (2019).

<sup>21</sup>D. Markauskas and R. Kacianauskas, “Investigation of rice grain flow by multi-sphere particle model with rolling resistance,” *Gran. Mat.* **13**, 143–148 (2011).

<sup>22</sup>S. D. Liu, Z. Y. Zhou, R. P. Zou, D. Pinson, and A. B. Yu, “Flow characteristics and discharge rate of ellipsoidal particles in a flat bottom hopper,” *Powder Technol.* **253**, 70–79 (2014).

<sup>23</sup>H. Tangri, Y. Guo, and J. S. Curtis, “Hopper discharge of elongated particles of varying aspect ratio: Experiments and dem simulations,” *Chem. Eng. Sci.* **4**, 100040 (2019).

<sup>24</sup>C. H. Rycroft, A. V. Orpe, and A. Kudrolli, *Phys. Rev. E* **80**, 031305 (2009).

<sup>25</sup>R. Arévalo and I. Zuriguel, “Clogging of granular materials in silos: effect of gravity and outlet size,” *Soft Matter* **12**, 123 (2016).

<sup>26</sup>L. E. Silbert, D. Ertas, G. S. Grest, T. C. Halsey, D. Levine, and S. J. Plimpton, “Granular flow down an inclined plane: Bagnold scaling and rheology,” *Phys. Rev. E* **64**, 051302 (2001).

<sup>27</sup>J. W. Landry, G. S. Grest, L. E. Silbert, and S. J. Plimpton, *Phys. Rev. E* **67**, 041303 (2003).